

Exploring the Properties and Potential of Single-crystal NCM 811 for Lithium-ion Batteries

Yongseok Lee¹ and Seunghoon Nam^{1,2,†}

¹Department of Materials Science and Engineering, College of Engineering, Andong National University, 1375, Gyeongdong-ro, Andong, Gyeongsangbuk-do, 36729, Republic of Korea

²Materials Research Centre for Energy and Clean Technology 1375, Gyeongdong-ro, Andong, Gyeongsangbuk-do, 36729, Republic of Korea

(Received January 20, 2023; Revised January 25, 2023; Accepted January 27, 2023)

Single-crystal Ni-rich NCM is a material that has drawn attention in the field of lithium-ion batteries due to its high energy density and long cycle life. In this study, we investigated the properties of single-crystal NCM 811 and its potential for use in lithium-ion batteries. High-quality single crystals of NCM 811 were successfully synthesized by crystal growth via a flux method. The single-crystal nature of the samples was confirmed through detailed characterization techniques, such as scanning electron microscopy and x-ray diffraction with Rietveld refinement. The crystal structure and electrochemical performances of the single-crystal NCM 811 were analyzed and compared to its poly-crystal counterpart. The results indicated that single-crystal NCM 811 had electrochemical performance and thermal stability superior to poly-crystalline NCM 811, making it a suitable candidate for high-performance batteries. The findings of this study contribute to a better understanding of the characteristics and potential of single-crystal NCM 811 for lithium-ion batteries.

Keywords: NCM 811, Flux Method, Single-Crystal NCM, Li-Ion Batteries

1. Introduction

Since the introduction of LiCoO₂ (LCO) as cathode materials commercialized in 1991, Li-ion batteries have long been used in power sources for various electronic devices and, in recent years, their roles have grown even to the transportation sector [1]. The crisis of global energy and Paris climate agreement pressured to change the existing infrastructure, and therefore, many countries evaluate electric vehicles (EVs) as one of the strategic emerging industries [2,3]. As a result, increasing demand for EVs with extended driving distance requires that Li-ion batteries for EVs be of higher energy density with safety and stable cycle-life [4,5]. The state-of-the-art cathodes for Li-ion batteries are a family of LiNiO₂ (LNO) by substitution of Ni with such elements as Co, Mn, and Al [6,7]. One of the subgroups is known as LiNi_xCo_yMn_{1-x-y}O₂ (NCM), in which Li and transition metals are positioned in the close-packed oxygen framework [8]. The NCM was investigated as a promising cathode material in the

early 2000s, as it can offer higher practical capacities than the conventional LCO at relatively lower voltages [6,7,9]. Since the capacity of NCM increases linearly with increasing Ni contents, the development of NCM is focused on so-called Ni-rich NCM where Ni composition is typically more than 0.6 [7,10].

Despite high theoretical capacities of Ni-rich NCMs (e. g. 278 mAh/g for NCM 811), these cathode materials show rapid fade of capacity, compared to the canonical LCO [11]. Many studies have been conducted on the degradation mechanisms, and likewise, various investigations were made to improve electrode stability [12]. It was shown that as the Ni content increases, intrinsic problems derived from LNO also occur in NCM, such as cation mixing, O₂ evolution, and particle cracking [12,13]. The cation mixing is one of the inherent defects of Ni-rich layered oxides caused by the similar ion radii of Ni²⁺ (0.69 Å) and Li⁺ (0.76 Å) [12]. According to the crystal field theory and Jahn-Teller effect, Ni ions tend to be reduced from Ni³⁺ to Ni²⁺ and at the same time, oxygen is released from the lattice only to generate O₂ [12,14].

In the meantime, particle cracking has also been considered one of the main issues for degradation of Ni-

[†]Corresponding author: shnam@anu.ac.kr

Seunghoon Nam: Professor, Yongseok Lee: M. S. Candidate

rich NCMs [12,13,15]. The degree of cracking becomes significant with higher Ni contents with abrupt change of c-lattice parameter due to the change in covalency between oxygen and transition metals during cycling [15,16]. For a poly-crystal NCM, cracks are generated mostly along the interparticle boundaries and hinder the mechanical integrity of the particles, leading to the loss of active material from the electrode substrate [15-17]. Suppressing the particle cracking is, therefore, a key factor to prevent the capacity fade from Ni-rich NCMs [13]. To minimize the capacity fade from particle cracking, growth of single-crystal NCMs can be a promising strategy [13,17,18]. By removing the interparticle boundaries, even Ni-rich NCMs would show improved capacity retention and thermal stability by minimizing parasitic surface degradation [16,18,19]. Furthermore, single-crystal NCMs have well-defined crystal structures, which can reduce the formation of defects and voids during the battery charging and discharging process, resulting in a lower rate of capacity fading and longer cycle life [18]. Higher rate performance of single-crystal NCMs is also an advantage attributed to faster lithium-ion diffusion [19]. This makes it particularly suitable for high-power applications such as electric vehicles and grid storage. Nevertheless, single-crystal Ni-rich NCMs are in the early stage of development with the synthetic methods still immature for the practical applications [18,20].

In this work, a single crystal of $\text{LiNi}_{0.8}\text{Co}_{0.1}\text{Mn}_{0.1}\text{O}_2$ (s-NCM) was successfully synthesized by a molten-salt flux method. With Na_2SO_4 as a flux solvent, the s-NCM showed regular morphology and uniform particle size, with better cycle-life performances than those of the poly-crystal $\text{LiNi}_{0.8}\text{Co}_{0.1}\text{Mn}_{0.1}\text{O}_2$ (p-NCM). The characteristics of the synthesized single-crystal NCM were corroborated by scanning electron microscopy (SEM) and x-ray diffraction with Rietveld refinement.

2. Experimental Methods

2.1 Materials Synthesis

The $\text{Ni}_{0.8}\text{Co}_{0.1}\text{Mn}_{0.1}(\text{OH})_2$ as a NCM precursor was prepared by a co-precipitation method. In detail, 4 M aqueous solution of $\text{NiSO}_4 \cdot 6\text{H}_2\text{O}$, $\text{CoSO}_4 \cdot 7\text{H}_2\text{O}$ and $\text{MnSO}_4 \cdot \text{H}_2\text{O}$ with a molar ratio of Ni : Co : Mn = 8:1:1, 2 M NaOH solution, and 2 M $\text{NH}_3 \cdot \text{H}_2\text{O}$ solution were

simultaneously injected into continuous stirred-tank reactor (CSTR). The NH_3 serves as a chelating agent to form aggregated secondary particles, and pH is carefully controlled to 11.2 throughout the reaction.

The resulting precipitates were washed with D.I. water, and dried in vacuum oven at 50 °C overnight. For the chemical lithiation, the precipitates were intimately mixed with $\text{LiOH} \cdot \text{H}_2\text{O}$ at a molar ratio of Li/TM = 1.05 and heat-treated in a tube furnace at 750 °C for 13 hours to obtain polycrystalline NCM811 (p-NCM). The single crystal NCM811 (s-NCM) was synthesized by adding Na_2SO_4 flux to the mixture. In the case of s-NCM, the ratio of Li/TM was set to be 1.1 to compensate lithium volatile in high-temperature heat treatment. The ratio of flux and solute was set to 8:2, and heat treatment was conducted at 900 °C for 13 hours. All the heat treatment processes were performed in an oxygen atmosphere, and samples obtained were filtered and washed with D.I. water.

2.2 Characterizations

The morphologies of obtained crystal products were identified using a scanning electron microscope (MIRA3 XMH, Tescan, Czech Republic). The elemental compositions were determined by electron probe micro analyzer (EPMA 1600, Shimadzu Corporation, Japan) and inductively coupled plasma spectrometer (Agilent-5110, Agilent, U.S.A.). The crystal structures were also identified using powder X-ray diffraction (Ultima IV, Rigaku, Japan) with Cu $K\alpha$ radiation at 25 kV. The diffraction was evaluated by a typical Rietveld refinement method. The battery electrodes were prepared with active materials, Super P carbon black, and polyvinylidene fluoride (PVDF) binder at a weight ratio of 90:5:5. The slurry was cast on Al foil, and dried overnight in a vacuum oven at 110 °C. All of the electrodes were assembled with 2032 type coin-cell in a glove box filled with Ar and Li-metal was used as both reference and counter electrodes. 1 M LiPF_6 in ethylene carbonate (EC) and dimethyl carbonate (DMC) (1:1 vol%) was used as an electrolyte (Panax Etec, Korea). The electrochemical cycling was performed using a galvanostatic charge/discharge within a cutoff voltage of 3.00 - 4.25 V (vs Li/Li⁺) at room temperature by a battery cycler (WBCS-3000, WonATech Co.Ltd, Korea).

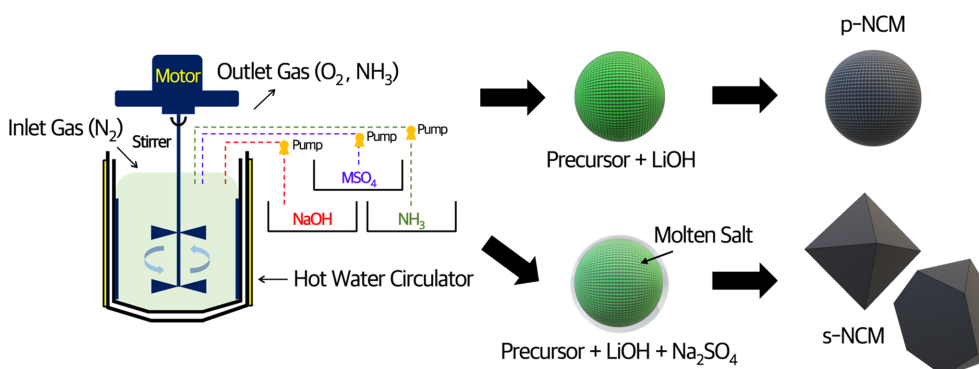


Fig. 1. An illustration of the synthetic procedures for s- and p-NCM particles. The initial NCM precursors are produced by coprecipitation reaction in a CSTR to guarantee homogenous elemental distribution of transition metals. Both s- and p-NCM are rendered by the addition of LiOH as a Li source, while Na_2SO_4 , as a molten salt, are included only to the synthesis of s-NCM

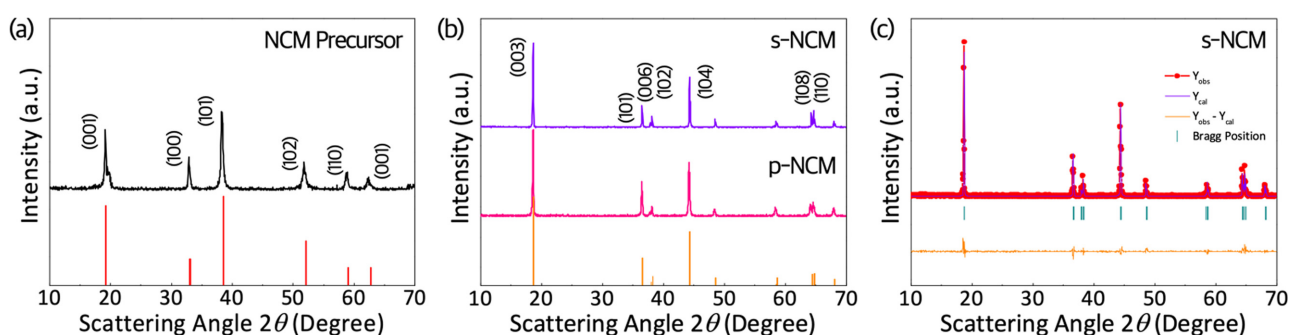


Fig. 2. X-ray diffraction of (a) $\text{Ni}_{0.8}\text{Co}_{0.1}\text{Mn}_{0.1}(\text{OH})_2$. Ideal peak positions and intensities are indicated for $\beta\text{-Ni}(\text{OH})_2$ (JCPDS #14-0117). (b) X-ray diffractions of s-NCM (single-crystal $\text{LiNi}_{0.8}\text{Co}_{0.1}\text{Mn}_{0.1}\text{O}_2$) and p-NCM (poly-crystal $\text{LiNi}_{0.8}\text{Co}_{0.1}\text{Mn}_{0.1}\text{O}_2$). Ideal peak positions and intensities are indicated for LiNiO_2 (JCPDS #09-0063). (c) Rietveld refinement of the diffraction of s-NCM

3. Results and Discussion

For the synthesis of s-NCM, NCM precursor ($\text{Ni}_{0.8}\text{Co}_{0.1}\text{Mn}_{0.1}(\text{OH})_2$) was produced by co-precipitation reaction in a continuously stirred tank reactor (CSTR, Fig. 1), followed by a flux-assisted sintering during which the NCM precursors and LiOH were dissolved in the Na_2SO_4 as a molten salt and supersaturation established either by cooling or reaction in the liquid phase. The synthetic route to s-NCM is briefly illustrated in Fig. 1.

From the previous studies, it is found out that increasing Ni content adversely affects the crystallinity of layered structure in NCM [21]. The degree of crystallinity is directly reflected in the cycle-life performance of NCM, in that diffusion of Li^+ is greatly influenced by atomic defects and crystal structure of the framework. Fig. 2 displays diffraction patterns of NCM precursor ($\text{Ni}_{0.8}\text{Co}_{0.1}\text{Mn}_{0.1}(\text{OH})_2$) with s- and p-NCMs. The precursors show diffracted peaks

corresponding to $\beta\text{-Ni}(\text{OH})_2$ with no obvious impurities. Both s- and p-NCM show typical diffraction of LiNiO_2 in the $R\bar{3}m$ space group, where splitting of (006)/(102) and (018)/(110) is quite distinct, indicative of highly-ordered layered structure. As can be seen in Fig. 2b, the intensity ratio of (003) and (104) diffraction of the s-NCM is higher than that of the p-NCM, showing (003)-oriented feature of s-NCM during the sample preparation for the x-ray diffraction, which could be an indication of single-crystalline phase. Even though the intensity ratio of (003) and (104) also a sign of the degree to which cation mixing occurs and s-NCM is heat-treated in higher temperature, the fact that the (003)/(104) ratio of s-NCM is higher than that of the p-NCM clearly shows the single crystal nature of s-NCM. In Fig. 2c, diffraction pattern of the s-NCM is refined by a Rietveld method, and detailed results are listed in Table 1. From the $Y_{\text{obs}} - Y_{\text{cal}}$ values from the Rietveld refinement, it can be seen that the s-NCM shows

Table 1. Details from Rietveld refinement from powder x-ray diffraction of s-NCM

Atom	Site	Wyckoff Positions			R $\bar{3}m$ Occupancy
Li	3a	0	0	0	0.00766
Ni	3a	0	0	0	0.06144
Co	3a	0	0	0	0.00812
Mn	3a	0	0	0	0.00834
Li	3b	0	0	1/2	0.08183
Ni	3b	0	0	1/2	0.00336
O	6c	0	0	0.25857	0.15698

$$a_{\text{hex}} = b_{\text{hex}} = 2.876112 \text{ \AA}, c_{\text{hex}} = 14.209514 \text{ \AA}$$

highly ordered layered structure.

Morphologies of the powders are clarified by scanning electron microscopy (SEM), as shown in Fig. 3. Fig. 3a is a SEM images of precursor, and Figs. 3b, c are images of p-NCM synthesized through a commercial heat treatment condition. From the Figs. 3a-c, it can be seen that the p-NCM follows the morphology of the precursor. It is observed that the particles of p-NCM exhibit spherical secondary particle ($\sim 10 \mu\text{m}$) formed by aggregation of polyhedron-shaped primary particles [22]. Figs. 3d-f show that size of the s-NCM particle is more or less $7 \mu\text{m}$ with well-developed octahedral single crystals as a result of

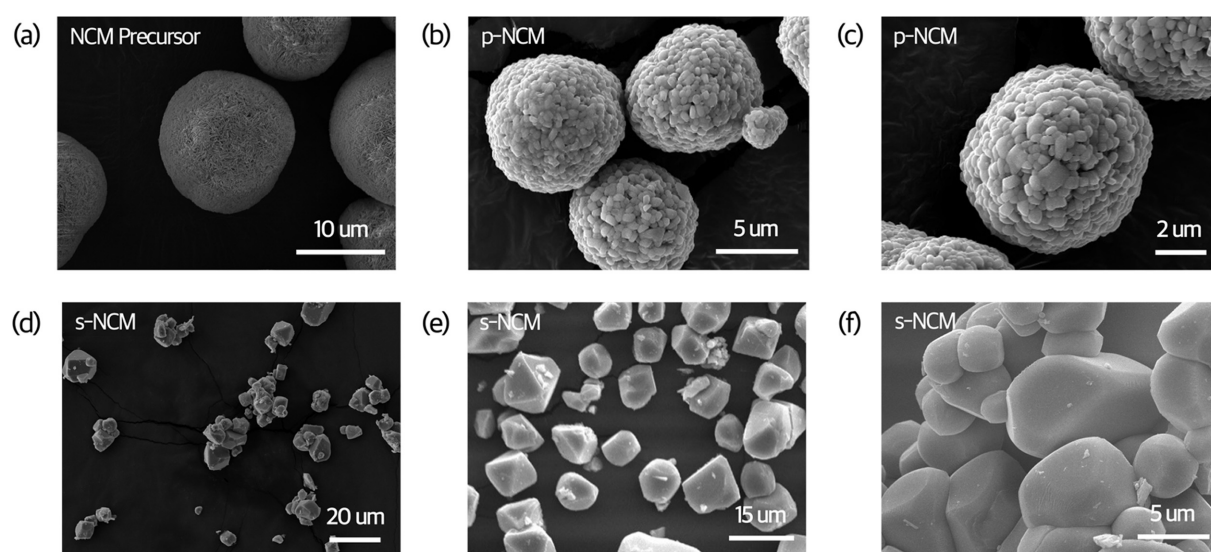


Fig. 3. A SEM image of (a) NCM precursor ($\text{Ni}_{0.8}\text{Co}_{0.1}\text{Mn}_{0.1}(\text{OH})_2$), SEM images of (b), (c) p-NCM (poly-crystal $\text{LiNi}_{0.8}\text{Co}_{0.1}\text{Mn}_{0.1}\text{O}_2$) and (d), (e), (f) s-NCM (single-crystal $\text{LiNi}_{0.8}\text{Co}_{0.1}\text{Mn}_{0.1}\text{O}_2$)

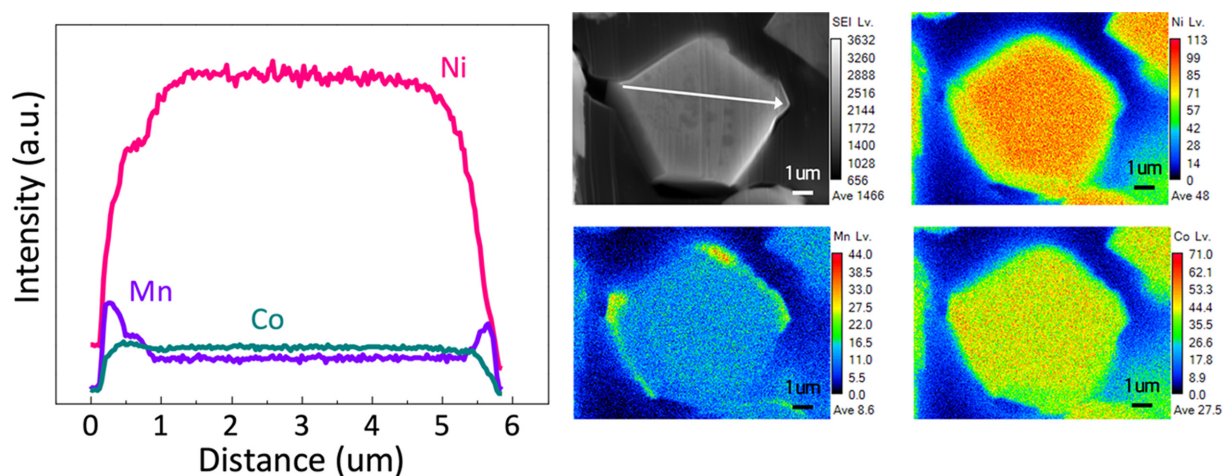


Fig. 4. EPMA result of a sliced s-NCM (single-crystal $\text{LiNi}_{0.8}\text{Co}_{0.1}\text{Mn}_{0.1}\text{O}_2$) particle by focused-ion beam (FIB) with elemental mapping of Ni, Mn, and Co, respectively. The position (distance) is indicated by an arrow in the figure

synthesis through the Na_2SO_4 flux method. Previous studies have shown that Na_2SO_4 flux has a significant impact on the creation of octahedron single crystals with rock salt structure in the $R\bar{3}m$ space group [20]. Others have identified that the form of these single crystals has better cycling stability with relatively-less gas evolution during (de)lithiation of s-NCM [20,23]. Takeshi *et al.* also mentioned that Na^+ ions in the flux can promote (003), (101), and (111) facets [20,23].

The elemental distribution in the s-NCM was identified by cross-sectional electron probe microanalysis (EPMA), as shown in Fig. 4. Despite some segregation of Mn species near the surface, the Ni, Mn, and Co elements are

uniformly distributed throughout the particle. As a result of line scan across the section of the single crystal, it can be observed that the ratio of transition metals is close to that of the precursor, in accordance with the inductively coupled plasma (ICP) analysis in Table 2.

CR2032 coin-cells using s-NCM and p-NCM as active materials were prepared, and their electrochemical performances were evaluated from 3.0 to 4.25 V at room temperature. For the battery formation, all of the cells were cycled at 20 mA/g (0.1 C, 1 C = 200 mAh/g, considering the practical capacity of NCM 811) for the first few cycles. Fig. 5 summarizes the fundamental electrochemical performances of NCM electrodes by

Table 2. The results of ICP analysis of the NCM precursor and s-NCM

Sample	Li (at.%)	Ni (at.%)	Mn (at.%)	Co (at.%)
NCM Precursor: $\text{Ni}_{0.8}\text{Co}_{0.1}\text{Mn}_{0.1}(\text{OH})_2$	-	79.50	10.37	10.13
s-NCM: $\text{LiNi}_{0.8}\text{Co}_{0.1}\text{Mn}_{0.1}\text{O}_2$	98.23	81.14	10.25	10.22

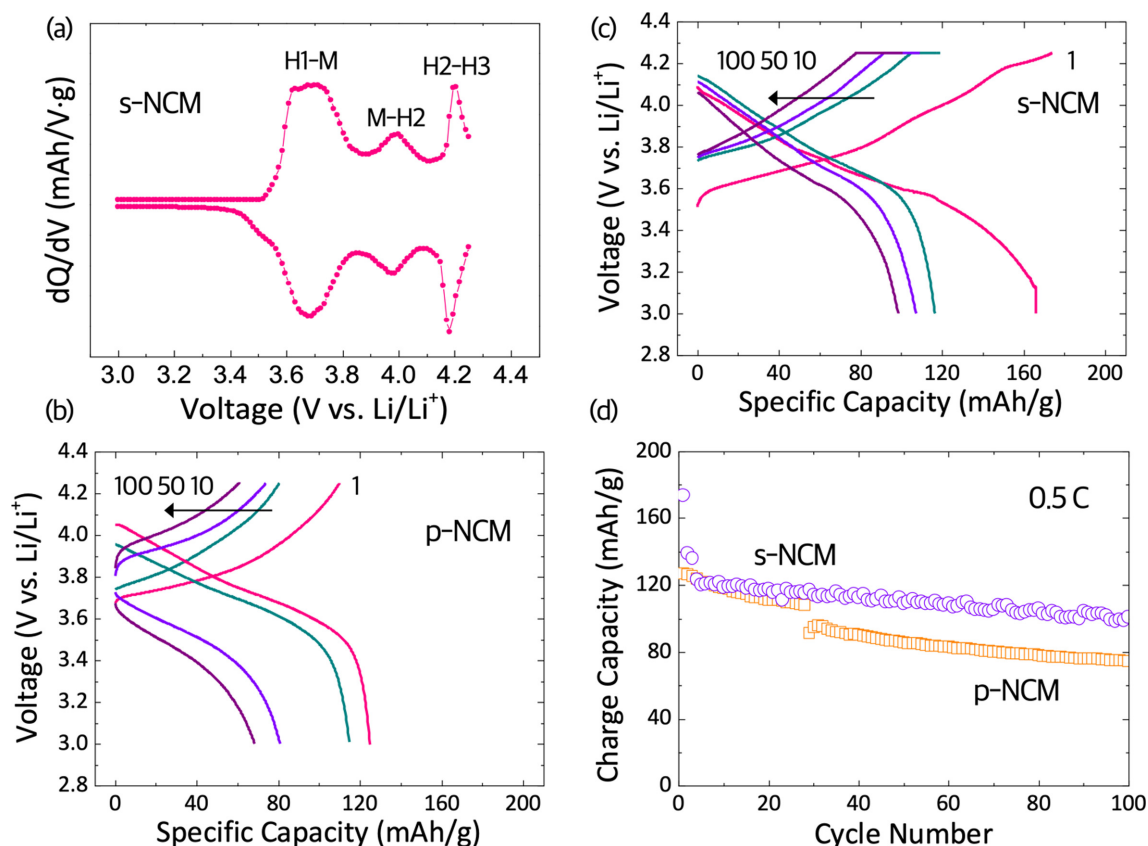


Fig. 5. (a) A dQ/dV curve of the s-NCM electrode at 0.5 C (1 C = 200 mAh/g). The peaks, indicative of various phase transitions, are marked in the figure. Galvanostatic charge/discharge profiles of (b) the p-NCM (poly-crystal $\text{LiNi}_{0.8}\text{Co}_{0.1}\text{Mn}_{0.1}\text{O}_2$) and (c) the s-NCM (single-crystal $\text{LiNi}_{0.8}\text{Co}_{0.1}\text{Mn}_{0.1}\text{O}_2$) at 0.5 C. Cycle-life performances of the s-NCM and p-NCM at the same C-rate. Note that the formation cycles are excluded

comparing s-NCM with p-NCM. Firstly, Fig. 5a shows a dQ/dV curve for the s-NCM electrode to reveal the phase transition behaviors during cycling [24]. Notably, O3 stacking sequence is preserved during the phase transitions of Ni-rich NCMs [25]. Individual phase that occurs in the phase transitions is labelled by a letter and number. Specifically, rhombohedral lattices are denoted as ‘H’ and the following numbers indicate the order in which each phase is observed on charge. Two-phase region is reflected as a plateau in a voltage profile, while it is depicted as a peak in differential capacity plot. Multiple peaks are observed in the dQ/dV curves of s-NCM, which corresponds to H1-M (monoclinic), M-H2, and H2-H3 phase coexistence. The process occurs reversibly during lithiation, indicating that the s-NCM shows high reversibility at the early stage of (de)lithiations. In the meantime, it is accepted that the phase transition from H2 to H3 results in lattice collapse through c-direction, thus the p-NCM would suffer from particle cracking during repetitive charge/discharges [15,16]. Fig. 5b and c show voltage profiles of 1st, 10th, 50th, and 100th cycle of the s- and p-NCM, respectively. The first charge capacity of the s-NCM amounts to ~170 mAh/g whereas that of the p-NCM only shows ~120 mAh/g. As expected, the decay of capacity is much severe for p-NCM, showing ~70 mAh/g after 100 cycles (Fig. 5d). The s-NCM displays, however, an excellent capacity retention even after 100 cycles. The difference in cyclability of the two samples is attributed to the resistance to particle cracking since p-NCM is more prone to particle cracks that would generate along the interparticle boundaries. The discontinuity caused by cracks leads to loss of active materials from electrode, and penetration of electrolyte into developed cracks, forming solid-electrolyte interphases. On the contrary, it seems that the s-NCM retains its morphology during the anisotropic lattice contraction/expansions, leading to better cycle-life performance than the p-NCM. For both s- and p-NCMs, degradation with increasing cycle numbers is inevitable, presumably due to cation mixing of Li/Ni and subsequent phase transformations to spinel or rock salt phases. Such cation mixing can be alleviated by surface coating with atomic layer deposition (ALD), doping aliovalent atoms to prevent Ni from migration, and etc, which would be one of the future works [26-28].

4. Conclusions

In conclusion, this study investigated the properties and potential of single crystal NCM 811 for lithium-ion batteries by comparing it to its polycrystalline counterpart. The results showed that the s-NCM exhibited superior electrochemical performance and thermal stability compared to polycrystalline NCM 811. The voltage profiles of s-NCM showed a higher voltage plateau and better reversibility, and the cycling tests revealed that s-NCM had a higher capacity retention and excellent cycle stability. These findings indicate that the s-NCM shows 1) a high level of electrochemical activity, 2) cycling stability, and 3) smaller irreversible capacity, making it a suitable candidate for high-performance lithium-ion batteries. The comparison between the two types of NCM 811 highlighted the advantages of the single crystal over the polycrystalline one. However, it is worth noting that the results were obtained by utilizing a specific synthesis method and condition, and further research is needed to optimize the material’s performance by conducting experiments with different synthesis methodologies.

Acknowledgments

This work was supported by a Research Grant of Andong National University.

References

1. Y. Chen, Y. Kang, Y. Zhao, L. Wang, J. Liu, Y. Li, Z. Liang, X. He, X. Li, N. Tavajohi, and B. Li, A review of lithium-ion battery safety concerns: The issues, strategies, and testing standards, *Journal of Energy Chemistry*, **59**, 83 (2021). Doi: <https://doi.org/10.1016/j.jechem.2020.10.017>
2. S. J. Hong, and S. Nam, Simple Synthesis of SiO_x by High-Energy Ball Milling as a Promising Anode Material for Li-Ion Batteries, *Corrosion Science and Technology*, **21**, 445 (2022). Doi: <https://doi.org/10.14773/cst.2022.21.6.445>
3. B. Song, W. Li, and A. Manthiram, A perspective on nickel-rich layered oxide cathodes for lithium-ion batteries, *Energy Storage Materials*, **6**, 125 (2017). Doi: <https://doi.org/10.1016/j.ensm.2016.10.007>
4. M. S. Whittingham, Lithium batteries and cathode materials, *Chemical Reviews*, **104**, 4271 (2004). Doi: <https://doi.org/10.1021/cr020731c>

5. D. Andre, S. Kim, P. Lamp, S. F. Lux, F. Maglia, O. Paschos, and B. Stiaszny, Future generation of cathode materials: an automotive industry perspective, *Journal of Materials Chemistry A*, **3**, 6709 (2015). Doi: <https://doi.org/10.1039/C5TA00361J>
6. R. V. Chebiam, A. M. Kannan, F. Prado, and A. Manthiram, Comparison of the chemical stability of the high energy density cathodes of lithium-ion batteries, *Electrochemistry Communications*, **3**, 624 (2001). Doi: [https://doi.org/10.1016/S1388-2481\(01\)00232-6](https://doi.org/10.1016/S1388-2481(01)00232-6)
7. A. Manthiram, B. Song, and W. Li, A perspective on nickel-rich layered oxide cathodes for lithium-ion batteries, *Energy Storage Materials*, **6**, 125 (2017). Doi: <https://doi.org/10.1016/j.ensm.2016.10.007>
8. M. Zhang, D. A. Kitchaev, Z. Lebens-Higgins, J. Vinckeviciute, M. Zuba, P. J. Reeves, C. P. Grey, Michael Stanley Whittingham, Louis F. J. Piper, Anton Van der Ven, and Y. Shirley Meng, Pushing the limit of 3d transition metal-based layered oxides that use both cation and anion redox for energy storage, *Nature Reviews Materials*, **7**, 522 (2022). Doi: <https://doi.org/10.1038/s41578-022-00416-1>
9. N. Nitta, F. Wu, J. T. Lee, G. Yushin, Li-ion battery materials: present and future, *Materials Today*, **18**, 5 (2015). Doi: <https://doi.org/10.1016/j.mattod.2014.10.040>
10. S.-H. Lee, S. Lee, B.-S. Jin & H.-S. Kim, Optimized electrochemical performance of Ni rich $\text{LiNi}_{0.91}\text{Co}_{0.06}\text{Mn}_{0.03}\text{O}_2$ cathodes for high-energy lithium ion batteries, *Scientific Reports*, **9**, 8901 (2019). Doi: <https://doi.org/10.1038/s41598-019-45531-2>
11. S. Jamil, G. Wang, M. Fasehullah, M. Xu, Challenges and prospects of nickel-rich layered oxide cathode material, *Journal of Alloys and Compounds*, **909**, 164727 (2022). Doi: <https://doi.org/10.1016/j.jallcom.2022.164727>
12. A. Chen, K. Wang, J. Li, Q. Mao, Z. Xiao, D. Zhu, G. Wang, P. Liao, J. He, Y. You, and Y. Xia, The Formation, Detriment and Solution of Residual Lithium Compounds on Ni-Rich Layered Oxides in Lithium-Ion Batteries, *Frontiers in Energy Research*, **8** (2020). Doi: <https://doi.org/10.3389/fenrg.2020.593009>
13. H.-H. Ryu, K.-J. Park, C. S. Yoon, and Y.-K. Sun, Capacity Fading of Ni-Rich $\text{Li}[\text{Ni}_x\text{Co}_y\text{Mn}_{1-x-y}]\text{O}_2$ ($0.6 \leq x \leq 0.95$) Cathodes for High-Energy-Density Lithium-Ion Batteries: Bulk or Surface Degradation?, *Chemistry of Materials*, **30**, 1155 (2018). Doi: <https://doi.org/10.1021/acs.chemmater.7b05269>
14. J.-H. Kim, H.-H. Ryu, S. J. Kim, C. S. Yoon, and Y.-K. Sun, Degradation Mechanism of Highly Ni-Rich $\text{Li}[\text{Ni}_x\text{Co}_y\text{Mn}_{1-x-y}]\text{O}_2$ Cathodes with $x > 0.9$, *ACS Applied Materials & Interfaces*, **11**, 30936 (2019). Doi: <https://doi.org/10.1021/acsami.9b09754>
15. H.-H. Sun, and A. Manthiram, Impact of Microcrack Generation and Surface Degradation on a Nickel-Rich Layered $\text{Li}[\text{Ni}_{0.9}\text{Co}_{0.05}]\text{O}_2$ Cathode for Lithium-Ion Batteries, *Chemistry of Materials*, **29**, 8486 (2017). Doi: <https://doi.org/10.1021/acs.chemmater.7b03268>
16. C. Liao, F. Li, and J. Liu, Challenges and Modification Strategies of Ni-Rich Cathode Materials Operating at High-Voltage, *Nanomaterials*, **12**, 1888 (2022). Doi: <https://doi.org/10.3390/nano12111888>
17. Y. Liang, H. Liu, G. Wang, C. Wang, Y. Ni, C.-W. Nan, L.-Z. Fan, Challenges, interface engineering, and processing strategies toward practical sulfide-based all-solid-state lithium batteries, *InfoMat*, **4**, 5 (2022). Doi: <https://doi.org/10.1002/inf2.12292>
18. X. Fan, G. Hu, B. Zhang, X. Ou, J. Zhang, W. Zhao, H. Jia, L. Zou, P. Li, Y. Yang, Crack-free single-crystalline Ni-rich layered NCM cathode enable superior cycling performance of lithium-ion batteries, *Nano Energy*, **70**, 104450 (2020). Doi: <https://doi.org/10.1016/j.nanoen.2020.104450>
19. S.-T. Myung, F. Maglia, K.-J. Park, C. S. Yoon, P. Lamp, S.-J. Kim, and Y.-K. Sun, Nickel-Rich Layered Cathode Materials for Automotive Lithium-Ion Batteries: Achievements and Perspectives, *ACS Energy Letters*, **2**, 196 (2016). Doi: <https://doi.org/10.1021/acsenergylett.6b00594>
20. T. Kimijima, N. Zettsu, and K. Teshima, Growth Manner of Octahedral-Shaped $\text{Li}(\text{Ni}_{1/3}\text{Co}_{1/3}\text{Mn}_{1/3})\text{O}_2$ Single Crystals in Molten Na_2SO_4 , *Crystal Growth & Design*, **16**, 2618 (2016). Doi: <https://doi.org/10.1021/acs.cgd.5b01723>
21. J. Zhu and G. Chen, Single-Crystal Based Studies for Correlating Properties and High-Voltage Performance of $\text{Li}[\text{Ni}_x\text{Mn}_y\text{Co}_{1-x-y}]\text{O}_2$ Cathodes, *Journal of Materials Chemistry A*, **7**, 5463 (2019). Doi: <https://doi.org/10.1039/C8TA10329A>
22. M.-H. Lee, Y.-J. Kang, S.-T. Myung, Y.-K. Sun, Synthetic optimization of $\text{Li}[\text{Ni}_{1/3}\text{Co}_{1/3}\text{Mn}_{1/3}]\text{O}_2$ via co-precipitation, *Electrochimica Acta*, **50**, 939 (2004). Doi: <https://doi.org/10.1016/j.electacta.2004.07.038>
23. Y. Kim, Lithium Nickel Cobalt Manganese Oxide Synthesized Using Alkali Chloride Flux : Morphology and Performance As a Cathode Material for Lithium Ion Batteries, *ACS Applied Materials & Interfaces*, **4**, 2329 (2012). Doi: <https://doi.org/10.1021/am300386j>
24. H. Zhu, Y. Tang, K. M. Wiaderek, O. J. Borkiewicz, Y.

- Ren, J. Zhang, J. Ren, L. Fan, C. C. Li, D. Li, X.-L. Wang, and Q. Liu, Spontaneous Strain Buffer Enables Superior Cycling Stability in Single-Crystal Nickel-Rich NCM Cathode, *Nano Letters*, **21**, 9997 (2021). Doi: <https://doi.org/10.1021/acs.nanolett.1c03613>
25. C. Xu, P. J. Reeves, Q. Jacquet, and C. P. Grey, Phase Behavior during Electrochemical Cycling of Ni-Rich Cathode Materials for Li-Ion Batteries, *Advanced Energy Materials*, **11**, 2003404 (2020). Doi: <https://doi.org/10.1002/aenm.202003404>
26. R. S. Negi, S. P. Culver, M. Wiche, S. Ahmed, K. Volz and M. T. Elm, Optimized atomic layer deposition of homogeneous, conductive Al₂O₃ coatings for high-nickel NCM containing ready-to-use electrodes, *Physical Chemistry and Chemical Physics*, **23**, 6725 (2021). Doi: <https://doi.org/10.1039/D0CP06422J>
27. B. Zhang, L. Cheng, P. Deng, Z. Xiao, L. Ming, Y. Zhao, B. Xu, J. Zhang, B. Wu, and X. Ou, Effects of transition metal doping on electrochemical properties of single-crystalline LiNi_{0.7}Co_{0.1}Mn_{0.2}O₂ cathode materials for lithium-ion batteries, *Journal of Alloys and Compounds*, **872**, 159619 (2021). Doi: <https://doi.org/10.1016/j.jallcom.2021.159619>
28. G.-T. Park, H.-H. Ryu, T.-C. Noh, G.-C. Kang, and Y.-K. Sun, Microstructure-optimized concentration-gradient NCM cathode for long-life Li-ion batteries, *Materials Today*, **52**, 9 (2022). Doi: <https://doi.org/10.1016/j.mat-tod.2021.11.01>